Critical Thresholds for CO2 Foam Generation in Homogeneous Porous Media

Tang, Jinyu; Wei, Bing; Yang, Mengke; Rossen, William R.

DOI
10.2118/218255-PA

Publication date
2025

Document Version
Final published version

Published in
SPE Journal

Critical Thresholds for CO_2 Foam Generation in Homogeneous Porous Media

Jinyu Tang[1,2*], Bing Wei[1*], Mengke Yang[1,3], and William R. Rossen[4]

[1]State Key Laboratory of Oil and Gas Reservoir Geology and Exploitation, Southwest Petroleum University
[2]Department of Chemical and Petroleum Engineering, United Arab Emirates University
[3]Now with Sinopec Southwest Oil & Gas Company
[4]Department of Geoscience and Engineering, Delft University of Technology

Summary

Long-distance propagation of foam is one key to deep gas mobility control for enhanced oil recovery and CO_2 sequestration. It depends on two processes—convection of bubbles and foam generation at the displacement front. Prior studies with N_2 foam show the existence of a critical threshold for foam generation in terms of a minimum pressure gradient $\nabla p_{\text{gen}}^{\text{min}}$ or minimum total interstitial velocity $v_{t,\text{gen}}^{\text{min}}$, beyond which strong-foam generation is triggered. The same mechanism controls foam propagation. There are few data for $\nabla p_{\text{gen}}^{\text{min}}$ or $v_{t,\text{gen}}^{\text{min}}$ for CO_2 foam.

We extend previous studies to quantify $\nabla p_{\text{gen}}^{\text{min}}$ and $v_{t,\text{gen}}^{\text{min}}$ for CO_2 foam generation and, for the first time, relate $\nabla p_{\text{gen}}^{\text{min}}$ and $v_{t,\text{gen}}^{\text{min}}$ to factors including injected quality (gas volume fraction in the fluids injected) f_g, surfactant concentration C_s, and permeability K. In each experiment, steady pressure gradient ∇p is measured at fixed injection rate and quality, with total interstitial velocity v_t increasing and then decreasing in a series of steps. The trigger for strong-foam generation features an abrupt jump in ∇p upon an increase in v_t.

In most cases, the data for ∇p as a function of v_t identify three regimes, which are coarse foam with low ∇p, an abrupt jump in ∇p, and strong foam with high ∇p. The abrupt jump in ∇p upon foam generation confirms the existence of $\nabla p_{\text{gen}}^{\text{min}}$ and $v_{t,\text{gen}}^{\text{min}}$ for CO_2 foam. We further show how $\nabla p_{\text{gen}}^{\text{min}}$ and $v_{t,\text{gen}}^{\text{min}}$ scale with f_g, C_s, and K. Conditions that stabilize lamellae reduce the values of the thresholds: Both $\nabla p_{\text{gen}}^{\text{min}}$ and $v_{t,\text{gen}}^{\text{min}}$ increase with f_g and decrease with increasing C_s or K. Specifically, $\nabla p_{\text{gen}}^{\text{min}}$ scales with f_g as $(f_g)^2$ and $v_{t,\text{gen}}^{\text{min}}$ scales as $(f_g)^4$, and both $\nabla p_{\text{gen}}^{\text{min}}$ and $v_{t,\text{gen}}^{\text{min}}$ scale with C_s as $(C_s)^{-0.4}$. The effect of K on the thresholds for foam generation is greater than the effects of f_g and C_s. Our data in artificial consolidated cores show that $\nabla p_{\text{gen}}^{\text{min}}$ scales with K as K^{-2} for CO_2 foam, in comparison with K^{-1} for N_2 foam in unconsolidated sand/bead packs. More data are needed to verify these correlations.

It is encouraging that $\nabla p_{\text{gen}}^{\text{min}}$ in the cores with K = 270 md or greater is less than 0.17 bar/m (~0.75 psi/ft), two to three orders of magnitude less than for N_2 foam. Such low $\nabla p_{\text{gen}}^{\text{min}}$ can be easily attainable throughout a formation. This suggests that limited ∇p deep in formations is much less of a restriction for long-distance propagation of CO_2 foam than for N_2 foam. Foam propagation could still be challenging in low-K reservoirs ($\nabla p_{\text{gen}}^{\text{min}}$ ~10 bar/m for K = 27 md). Nevertheless, formation heterogeneity and alternating slug injection of gas and liquid help foam generation and can reduce the values of $\nabla p_{\text{gen}}^{\text{min}}$. More research is needed to predict long-distance propagation of foam at low ∇p and v_t.

Introduction

Gas injection into geological formations is often subject to poor volumetric sweep efficiency (Rossen 1996). This results from gravity segregation (due to lower gas density than liquids), gas fingering (due to greater gas mobility than liquids), and channeling (due to formation heterogeneity). Foam is currently the most effective means for gas sweep improvement, as it can reduce gas mobility considerably (e.g., by a factor of 10–10^4). This unique feature allows foam to have a broad range of applications in various subsurface processes, such as enhanced oil recovery, acid diversion in well stimulation, and soil/aquifer remediation. Foam can also be a promising means for geological carbon sequestration, benefiting both improved sweep and safe trapping of CO_2 in place (Rognmo et al. 2018; Rossen et al. 2024).

Foam can be easily created in the vicinity of an injection well, where pressure gradient and velocity are high. For this foam to propagate deep into the formation, it must propagate away from the injection well at low pressure gradient and superficial velocity. Long-distance propagation of foam is driven by two simultaneous processes—convection of bubbles generated upstream and generation of new bubbles at the displacement front. One key issue concerns the conditions for delivering foam deep into a formation at low pressure gradient and low superficial velocity. Reported data for N_2 foam show the existence of a minimum pressure gradient ($\nabla p_{\text{gen}}^{\text{min}}$) or minimum total interstitial velocity ($v_{t,\text{gen}}^{\text{min}}$) beyond which foam generation is possible (Gauglitz et al. 2002). The minimum pressure gradient/velocity for foam propagation depends on similar mechanisms, though for propagation, the minimum pressure gradient is greater, and the minimum velocity less, than those for generation (Ashoori et al. 2012; Yu et al. 2020). In many cases with N_2, observed values of $\nabla p_{\text{gen}}^{\text{min}}$ or $v_{t,\text{gen}}^{\text{min}}$ (Yu et al. 2020) are much too high to be seen in the field. This suggests that long-distance propagation of N_2 foam could be challenging. However, there are few data available in the literature for CO_2 foam (Gauglitz et al. 2002). With supercritical CO_2, one may expect lower $\nabla p_{\text{gen}}^{\text{min}}$ or $v_{t,\text{gen}}^{\text{min}}$, partly because surface tension for supercritical CO_2-water is lower than for N_2-water. Nevertheless, the quantitative conditions for the generation and propagation of CO_2 foam in porous rocks are unclear due to the lack of relevant data. This poses a large uncertainty in evaluating the feasibility and potential of foam for large-scale carbon sequestration, particularly under low-pressure gradient/low-velocity conditions away from an injection well.

*Corresponding author; email: bwei@swpu.edu.cn; j.tang@uaeu.ac.ae

This paper (SPE 218255) was accepted for presentation at the SPE Improved Oil Recovery Conference, Tulsa, Oklahoma, USA, 22–25 April 2024, and revised for publication. Original SPE manuscript received for review 12 July 2024. Revised manuscript received for review 14 October 2024. Paper peer approved 15 October 2024.

The goal of the study is to quantify the conditions of ∇p_{gen}^{min} and $v_{t,gen}^{min}$ required for CO_2 foam generation in homogeneous porous media. Furthermore, we correlate ∇p_{gen}^{min} and $v_{t,gen}^{min}$ with injected quality (volumetric fraction of gas in the fluids injected, f_g), surfactant concentration (C_s), and medium permeability (K). Other factors, such as heterogeneity and alternate slug injection of gas and liquid, also help foam generation. We examine steady gas/liquid injection through homogeneous, artificial consolidated cores for simplicity in this initial study. The measured data for ∇p_{gen}^{min} and $v_{t,gen}^{min}$ reveal the mechanisms and conditions triggering CO_2 foam generation. Incorporating the physics of foam generation and propagation thresholds into simulations is crucial to evaluating the feasibility of, or optimizing the design of, field projects that require deep CO_2-foam propagation. The data reported in this study could be used to fit model parameters for field-scale simulation of foam injection processes.

Brief Review of Foam Generation in Porous Media

Foam generation is the creation of "strong" foam, with a large increase in pressure gradient (∇p) and apparent viscosity (μ_{app}; i.e., the inverse of total relative mobility of gas and liquid) from a state of no-foam or "coarse" foam, with little or no mobility reduction. This transition depends on creation and accumulation of lamellae (i.e., thin liquid films separating bubbles; Rossen and Gauglitz 1990). Thus, foam generation is related to, but not identical to, lamella creation. It requires that the lamella creation rate be greater than the destruction rate. This means that the stability of lamellae is crucial, given that many factors (e.g., most crude oils) may destabilize foam (Farajzadeh et al. 2012; Tang et al. 2019a, 2019b).

Mechanisms of Lamella Creation. Four mechanisms have been identified for lamella creation (Ransohoff and Radke 1988; Rossen 1996, 2003). (1) "Leave behind" creates lamellae by means of gas invasion into a medium initially saturated with water. (2) "Snap-off" creates lamellae in pore throats, where water films bridge throats at sufficiently low capillary pressure. (3) "Lamella division" creates new lamellae when a lamella is forced through a pore body connected to several pore throats. Lamella division requires a sufficient pressure gradient to mobilize the lamella through pore throats. (4) "Gas evolution within liquid" creates foam when gas is generated in a surfactant solution.

Foam Generation at Fixed Quality. After a period of steady gas/liquid injection, the creation of strong foam at the same quality depends on injection rate and pressure gradient. With increasing total superficial velocity at a constant quality, the transition from no/coarse foam to strong foam features an abrupt, large increase in ∇p and μ_{app}. Both theory and laboratory data show that, for fixed injected quality, a plot of ∇p or μ_{app} as a function of total superficial velocity forms an S-shaped curve (Kam 2008; see also Fig. 16 in Gauglitz et al. 2002). The curve is reminiscent of catastrophe theory (Zeeman 1977), nowadays known as bifurcation theory.

Fig. 1a represents the process of foam generation in terms of the response of total interstitial velocity v_t as a function of ∇p. Three foam regimes are identified as the lower, coarse-foam regime with low ∇p; the upper, strong-foam regime with high ∇p; and the intermediate foam regime with ∇p between the other two regimes. As stated in catastrophe theory, the intermediate regime is intrinsically unstable (no tolerance to perturbations in ∇p or v_t); this was observed experimentally by Gauglitz et al. (2002). As a result, foam states in the intermediate unstable regime cannot be observed naturally.

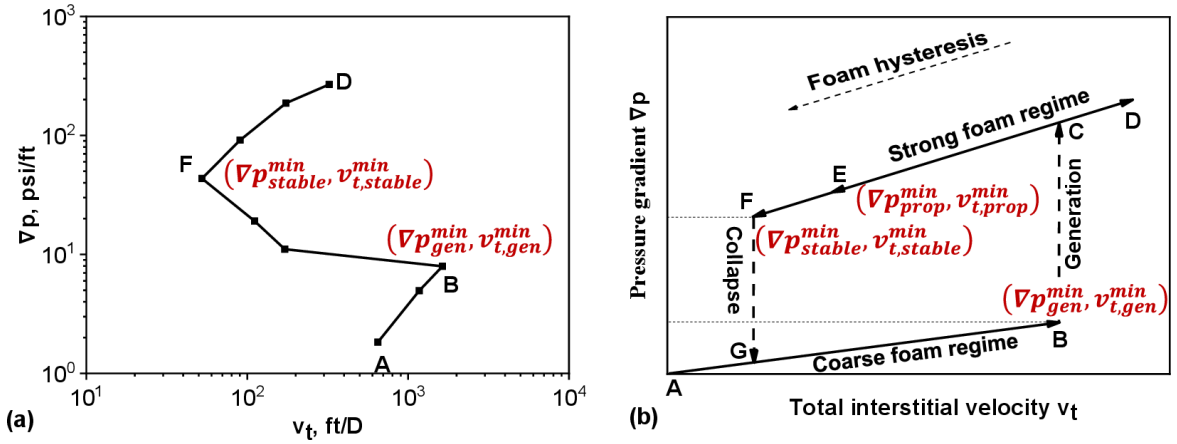

Fig. 1—Foam generation as a function of pressure gradient ∇p (left figure) or of total interstitial velocity v_t (right figure): (a) v_t measured as a function of ∇p in a sequence of increasing ∇p following A-B-F-D (Gauglitz et al. 2002) and (b) schematic of ∇p measured as a function of v_t in a sequence of increasing and then decreasing v_t following A-B-C-D-E-F-G (Yu et al. 2020). The letter labels in Fig. 1a correspond to those in Fig. 1b. Fig. 1a is N_2 foam data in Boise sandstone of 7.1 darcies (after Gauglitz et al. 2002).

The data in **Fig. 1a** were obtained by measuring gas and liquid rates at a constant quality f_g in steady-state corefloods, where ∇p across a core was fixed in each measurement and raised in steps. With increasing ∇p from Point A to Point B, foam is coarse, and velocities of gas (u_g) and liquid (u_w) must increase to meet the preset ∇p in each step. Thereafter, foam enters the intermediate regime where the curve folds back toward lower velocities. This is because the population of lamellae rises with ∇p to an extent that the reduction in gas mobility is more than the increase in ∇p. As a result, lower total interstitial velocity is needed to maintain the fixed ∇p, causing the curve to fold back. Although the intermediate regime was observed, maintaining both fixed ∇p and f_g was very difficult, consistent with its unstable nature as predicted by the catastrophe theory. Starting from Point F, the curve folds forward again, entering the strong-foam regime with v_t increasing with ∇p.

In the literature, most studies examine foam generation using fixed injection rate instead of fixed ∇p. **Fig. 1b** schematically illustrates the process of foam generation in terms of ∇p measured as a function of fixed total interstitial velocity v_t. With increasing v_t, ∇p makes

an abrupt, upward jump upon foam generation. The onset of the upward jump marks the minimum pressure gradient, $\nabla p_{\text{gen}}^{\text{min}}$ (Point B), and the corresponding minimum total interstitial velocity, $v_{t,\text{gen}}^{\text{min}}$, for triggering strong foam. With sufficient decrease in v_t, ∇p makes an abrupt, downward jump, meaning abrupt foam collapse. The onset of the downward jump indicates a minimum pressure gradient $\nabla p_{\text{stable}}^{\text{min}}$ (Point F) and the corresponding minimum total interstitial velocity $v_{t,\text{stable}}^{\text{min}}$ for maintaining a stable foam (Yu et al. 2020). The data of Yu et al. (2020) with N_2 in a 2.5-darcy Bentheimer sandstone core also show the existence of a minimum pressure gradient and minimum total interstitial velocity for foam propagation, $\nabla p_{\text{prop}}^{\text{min}}$ and $v_{t,\text{prop}}^{\text{min}}$ (Point E). Below this critical value, foam is maintained in place but does not propagate forward.

The critical thresholds for foam generation, stability, and propagation follow the relation: $\nabla p_{\text{prop}}^{\text{min}} > \nabla p_{\text{stable}}^{\text{min}} >> \nabla p_{\text{gen}}^{\text{min}}$, with $v_{t,\text{gen}}^{\text{min}} >> v_{t,\text{prop}}^{\text{min}} > v_{t,\text{stable}}^{\text{min}}$. This suggests that, at low pressure gradients, foam propagation is more challenging than triggering the transition to greatly reduced gas mobility. The conditions for foam propagation depend on the same mechanisms as foam generation, however (Ashoori et al. 2012; Yu and Rossen 2022).

Correlations between $\nabla p_{\text{gen}}^{\text{min}}$ and K. Very few studies in the literature address the quantitative correlations between $\nabla p_{\text{gen}}^{\text{min}}$ and K (e.g., Rossen and Gauglitz 1990; Chou 1991; Gauglitz et al. 2002; Lotfollahi et al. 2017). Most data obtained for fitting those correlations are with N_2. Only a few data are available with CO_2; the data of Gauglitz et al. span one order of magnitude in K for Boise sandstone. Given the lack of sufficient data, the quantitative correlations between $\nabla p_{\text{gen}}^{\text{min}}$ and influential factors were unknown for CO_2 foam.

In agreement with the percolation theory of Rossen and Gauglitz (1990), Gauglitz et al. (2002) find that $\nabla p_{\text{gen}}^{\text{min}}$ scales with medium permeability as K^{-1} for unconsolidated porous media:

$$\nabla p_{\text{gen}}^{\text{min}} \sim K^{-1}. \tag{1}$$

Eq. 1 is based on the pressure difference across an individual liquid lens, incorporating the impact of pore geometry. It also assumes that pore length and pore throat diameter each scale as $K^{-1/2}$, a reasonable assumption for unconsolidated bead and grain packs.

Ransohoff and Radke (1988) present a critical capillary number of 8 for generation, using the definition of

$$N_c \equiv \frac{\mu_{nw} v_t \varphi L R_g}{\sigma K K_{rnw}} = \frac{\nabla p L R_g}{f_{nw} \sigma}, \tag{2}$$

where μ_{nw} is the viscosity of the nonwetting phase (gas here), v_t is the total interstitial velocity, φ is the medium porosity, L is the medium length, R_g is the rock grain radius, σ is the surface tension, K is the permeability, K_{rnw} is the nonwetting-phase relative permeability, ∇p is the pressure gradient across the medium, f_{nw} is the nonwetting-phase fraction. Gauglitz et al. (2002) convert the left equation to the right one using Darcy's law for gas phase. Then, substituting $N_{ca} = 8$ into the right side of Eq. 2 converts the critical capillary number to $\nabla p_{\text{gen}}^{\text{min}}$:

$$\nabla p_{\text{gen}}^{\text{min}} = \frac{8 f_{nw} \sigma}{L} \sqrt{\frac{4\varphi^3}{150 K (1-\varphi)^2}}. \tag{3}$$

However, the $\nabla p_{\text{gen}}^{\text{min}}$ data of Ransohoff and Radke (1988) actually reflect the capillary end effect and capillary entry pressure, not directly the minimum pressure gradient required for foam generation (Rossen 2003).

Tanzil et al. (2000, 2002) report a critical capillary number of 2 for foam generation, using the definition:

$$N_c \equiv \frac{\Delta p}{\sigma} \sqrt{\frac{K}{\varphi}} = 2, \tag{4}$$

where the parameters here have the same definitions as in Eq. 2. Gauglitz et al. (2002) convert Eq. 4 to a minimum pressure gradient, through the Blake-Kozeny correlation for K (Bird et al. 2002):

$$\nabla p_{\text{gen}}^{\text{min}} = \frac{2\sigma}{L} \sqrt{\frac{\varphi}{K}}, \tag{5}$$

where L is the length of the medium. However, the experiments of Tanzil et al. (2000, 2002) were conducted in a drainage process, not at steady state.

Experimental Methodology

Fig. 2 shows a schematic of the coreflood apparatus used in our study. The whole setup was placed in an oven except for the pumps and data-recording system. We used dual ISCO pumps to allow for continuous coinjection of gas and liquid that were stored in respective transfer vessels. A Hassler core holder was used and mounted vertically, with fluids injected from the top, to avoid gravity segregation. Two absolute pressure transducers of accuracy ±0.01 bar are used to measure overall pressure drops across the core. Pressure (p) in the system was controlled by means of a backpressure regulator (abbreviated BPR in the figure) with accuracy ±1 bar. Pressure taps were located 1 cm from the inlet and outlet, respectively, to minimize entrance and exit effects in the ∇p data.

For the purpose of the study, we examined permeabilities K in the range of 10–10^3 md, injected quality f_g from 0.5 to 0.9, and different surfactant concentrations C_s. All our experiments were conducted at 40°C with a backpressure of 80 bar, with CO_2 in the supercritical

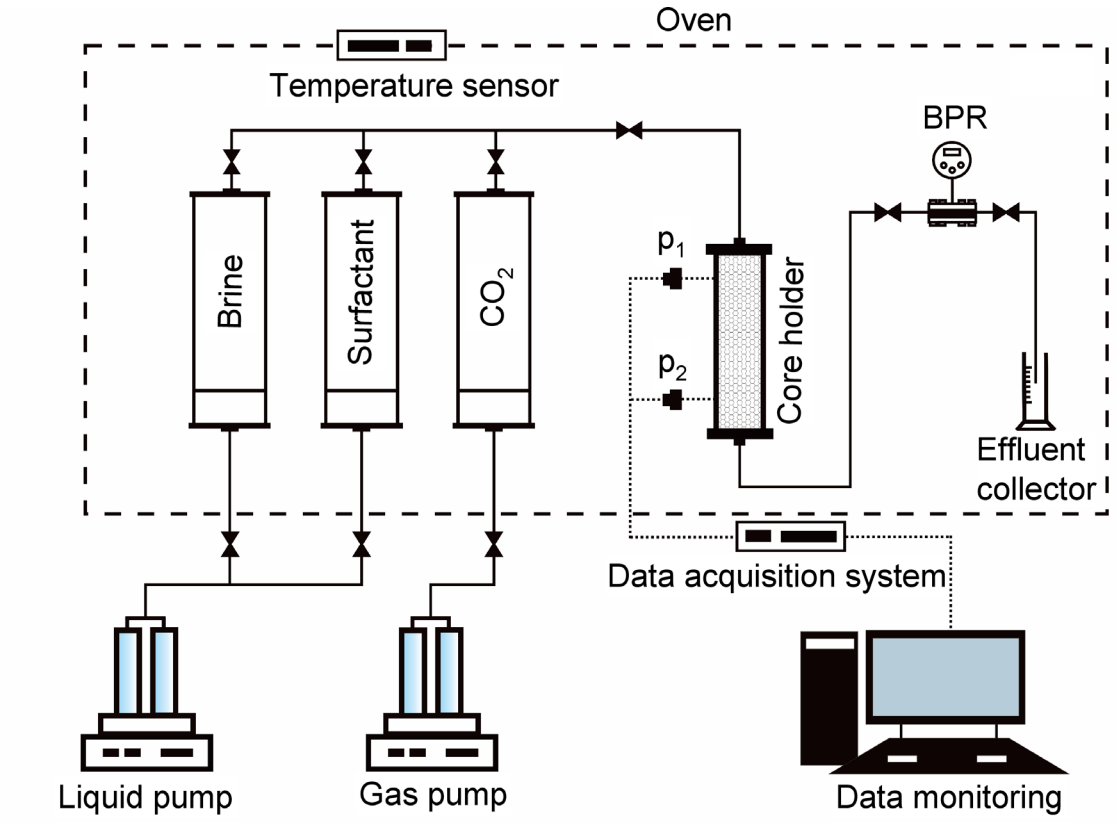

Fig. 2—Schematic of the coreflood apparatus for foam generation process at fixed injection rates. The whole setup is placed inside an oven except for injection pumps and data collection system.

state. The oven was set at 50°C, while the oven temperature (measured using a thermometer) was 40°C. Before foam injection, each core was flushed with 4 PV of surfactant solution to satisfy surfactant adsorption. The quality f_g was fixed in each experiment, and gas and liquid were coinjected following the v_t sequence as in **Fig. 1b**: increase v_t in steps through a few points after strong foam was observed and then reduce v_t to the initial value. ∇p was recorded with time for each v_t. To ensure steady-state and uniform surfactant concentration, at least 2 PV of surfactant solution were injected in each measurement.

Table 1 lists the experimental materials and properties of the rock and fluids. We use artificial consolidated, homogeneous sandstone cores (Al-Homadhi 2002; Jishun 2004; Wang et al. 2012) from Tiandi Science & Technology in China. All the cores are water-wet with a contact angle of about 69° in a supercritical CO_2-brine-rock system at 40°C and 80 bar. The relative permeability functions for water and gas without foam are those measured in homogeneous Bentheimer sandstone (Eftekhari and Farajzadeh 2017). The foaming agent used was APG0814, a nonionic surfactant from Shanghai Acmec Biochemical in China. Its chemical formula is $(C_6H_{11}O_5)_n$ OR, where n = 8–14 with a linear hydrocarbon chain and R denotes the Alkyl group. We also measured supercritical CO_2-surfactant surface tension σ at different values of C_s, using a pendant-drop tensiometer, DSA100HP690, from KRÜSS Scientific in Hamburg, Germany. The data indicate a critical micelle concentration (CMC) of 0.09 wt%.

Materials	Properties
Artificial consolidated sandstone cores	D = 2.5 cm and L = 8 cm K_1 = 27 md, φ_1 = 0.17 K_2 = 274 md, φ_2 = 0.21 K_3 = 905 md, φ_3 = 0.24 Water-wet
CO_2	μ_g = 0.03 cp
Brine, 3 wt% NaCl	μ_w = 0.7 cp
Water relative permeability	$K_{rw}(S_w) = 0.713\left(\frac{S_w-0.135}{0.665}\right)^{2.46}$
Gas relative permeability without foam	$K_{rg}^{nf}(S_g) = 0.94\left(\frac{S_g-0.2}{0.665}\right)^{1.3}$

Table 1—Rock and fluid properties at the experimental conditions T = 40°C and p = 80 bar.

Materials	Properties
Surfactant APG0814*	σ = 2.82 mN/m at C_s = 1 wt% σ = 2.87 mN/m at C_s = 0.5 wt% σ = 2.96 mN/m at C_s = 0.1 wt% σ = 4.26 mN/m at C_s = 0.05 wt% σ = 10.70 mN/m at C_s = 0.01 wt% σ = 12.91 mN/m at C_s = 0 wt%

*σ was measured at T = 50°C and p = 80 bar with a precision of ±0.01 mN/m.

Table 1 (continued)—Rock and fluid properties at the experimental conditions T = 40°C and p = 80 bar.

Experimental Results

Determination of ∇p_{gen}^{min} and $v_{t,gen}^{min}$ for CO_2 Foam. Fig. 3 shows our data for ∇p_{gen}^{min} measured at constant injected f_g = 0.6 with C_s = 0.5 wt% in the 905-md core. Arrows indicate the increasing and then decreasing velocity sequence where ∇p is measured. All the experiments in our study follow the same v_t sequence.

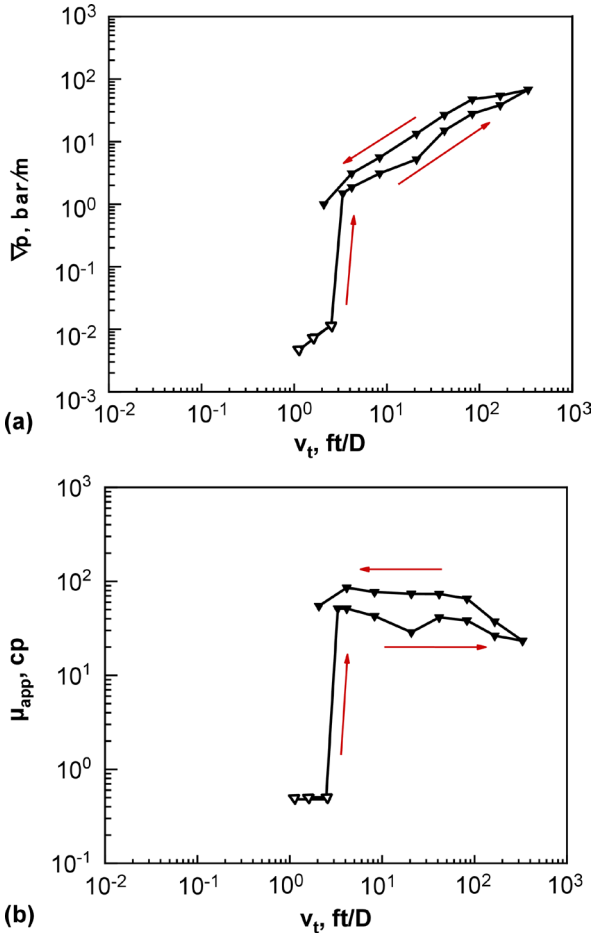

Fig. 3—(a) Pressure gradient ∇p (bar/m) and (b) apparent viscosity μ_{app} (cp) as a function of total interstitial velocity v_t (ft/D) in the 905-md core, respectively. Each symbol represents a steady measurement at constant f_g = 0.6 with C_s = 0.5 wt%, except for open symbols denoting values estimated from Darcy's law, as ∇p for those points was below the resolution of our apparatus. Arrows indicate the v_t sequence imposed.

In this case and some cases below, ∇p is too low to be measurable at low velocities in our experiments. Gauglitz et al. (2002) show that in a Boise core of 950 md, ∇p for coarse CO_2 foam is almost the same as CO_2-water injection without foam. We then estimate those low ∇p values based on Darcy's law for gas/liquid injection without foam, which are denoted by open symbols in **Fig. 3**. In the absence of foam, quality f_g is defined as

$$f_g = \frac{k_{rg}^{nf}/\mu_g}{k_{rw}/\mu_w + k_{rg}^{nf}/\mu_g}, \quad (6)$$

which is a function of water and gas saturations. By substituting the relative permeability functions in **Table 1** into Eq. 6, one can calculate gas and water saturations at $f_g = 0.6$. Then, one can calculate the corresponding ∇p at a given v_t without foam, based on total superficial velocity ($v_t \times \varphi$).

At low v_t, ∇p is very low. As v_t increases to $v_{t,\text{gen}}^{\min}$, ∇p, as seen from **Fig. 3a**, jumps upward abruptly by two orders of magnitude, marking the onset of strong-foam generation. The value of ∇p estimated just before the jump approximates the value of $\nabla p_{\text{gen}}^{\min}$ (Point B in **Fig. 1**) for triggering strong foam. In **Fig. 3a**, $\nabla p_{\text{gen}}^{\min}$ is ~0.01 bar/m (~0.04 psi/ft), very easily attainable throughout the formation during foam injection. This value is about two orders of magnitude less than for N_2 foam [e.g., $\nabla p_{\text{gen}}^{\min} \sim 4.52$ bar/m (20 psi/ft) at $f_g = 0.88$ in a 2.5-darcy Bentheimer sandstone core (Yu et al. 2020)]. The considerable difference in $\nabla p_{\text{gen}}^{\min}$ values demonstrates that deep in a formation, where ∇p is low, foam generation is a restriction to the long-distance propagation of N_2 foam but is much less an issue for CO_2 foam.

The minimum total interstitial velocity $v_{t,\text{gen}}^{\min}$ and minimum pressure gradient $\nabla p_{\text{gen}}^{\min}$ are related by Darcy's law:

$$v_{t,\text{gen}}^{\min} = \frac{1}{\varphi} K \lambda_{rt} \nabla p_{\text{gen}}^{\min}, \tag{7}$$

where

$$\lambda_{rt} = \frac{k_{rw}}{\mu_w} + \frac{k_{rg}^f}{\mu_g}, \tag{8}$$

with λ_{rt} being the total relative mobility and the k_{rg}^f denoting the effective gas relative permeability with foam. Although we set injection rate and measure ∇p, $\nabla p_{\text{gen}}^{\min}$ is the key for foam generation; $v_{t,\text{gen}}^{\min}$ is the velocity needed to meet the required value of $\nabla p_{\text{gen}}^{\min}$. This is because the mechanisms of lamella creation occur in a mobilization process, driven by pressure gradient.

Although the triggering of strong foam requires a velocity above $v_{t,\text{gen}}^{\min}$, the strong foam generated can be maintained at velocities below $v_{t,\text{gen}}^{\min}$. The mobility in the strong-foam regime is much lower than in the coarse-foam regime at same velocities. Thus, maintaining a strong foam requires a pressure gradient much greater than $\nabla p_{\text{gen}}^{\min}$ but a velocity lower than $v_{t,\text{gen}}^{\min}$. Since the injection rates examined in the decreasing sequence were not low enough, we could not determine the exact value of the minimum pressure gradient $\nabla p_{\text{stable}}^{\min}$ (Point F in **Fig. 1**) for maintaining a stable foam. However, its value would be less than 1 bar/m (4.2 psi/ft), the last measured datum, which is one to two orders of magnitude less than for N_2 foam (Yu et al. 2020). Their data with N_2 also show that the value of $\nabla p_{\text{prop}}^{\min}$ for foam propagation is greater than $\nabla p_{\text{stable}}^{\min}$ for maintaining its stability and much greater than $\nabla p_{\text{gen}}^{\min}$ for triggering its generation. More research is needed to quantify the conditions of $\nabla p_{\text{stable}}^{\min}$ and $\nabla p_{\text{prop}}^{\min}$ for CO_2 foam.

We also show foam apparent viscosity associated with the ∇p data, defined as

$$\mu_{\text{app}} \equiv \frac{1}{\lambda_{rt}}. \tag{9}$$

As seen in **Fig. 3b**, apparent viscosity μ_{app} at $\nabla p_{\text{gen}}^{\min}$, consistent with the ∇p response, jumps abruptly from 0.49 cp to 49 cp, and foam generation erupts everywhere along the core. This indicates that foam enters the strong regime. Foam strength (μ_{app}) in the decreasing v_t sequence is greater than in the increasing v_t sequence, exhibiting a 40–80% hysteresis in μ_{app} between the two sequences. This suggests that even within the strong-foam regime, the final state depends, in part, on the previous foam state; the exact cause is not clear when, as here, both states exhibit strong foam. In addition, foam in the strong-foam regime appears to be shear-thinning for both increasing and decreasing v_t: μ_{app} falls by a factor of ~2 over a 100-fold increase in v_t.

Effect of Injected Quality. The percolation theory of Rossen and Gauglitz (1990) predicts that foam generation shows a dependence on injected quality f_g—increasing $v_{t,\text{gen}}^{\min}$ with increasing f_g. Their data and those in Kam and Rossen (2002) and Yu et al. (2020) experimentally validate this dependence for N_2 foam. Here, we show the effect of f_g on CO_2 foam generation and quantify the correlations between $\nabla p_{\text{gen}}^{\min}$, $v_{t,\text{gen}}^{\min}$, and f_g.

We measured $\nabla p_{\text{gen}}^{\min}$ as a function of f_g in cores of permeabilities 905 md, 274 md, and 27 md. Field selection of injected f_g depends on many factors, including chemical cost (amount of surfactant injected) and effectiveness of mobility control with strong foam. Here, we examine the effect of f_g in the range of 0.5–0.9.

Fig. 4a displays the $\nabla p_{\text{gen}}^{\min}$ measurements for f_g ranging from 0.5 to 0.9 in the 905-md core. The values of ∇p before foam generation are triggered could not be measured, denoted by the open symbols; it is estimated from v_t based on Darcy's law. The data suggest that the values of $\nabla p_{\text{gen}}^{\min}$ rise with increasing f_g by a factor about 4, falling within the range of 10^{-3}–10^{-2} bar/m (0.004–0.04 psi/ft). ∇p in the field could easily exceed such low $\nabla p_{\text{gen}}^{\min}$. The equivalent $v_{t,\text{gen}}^{\min}$ values also increase with f_g but by a factor about 10. As seen from Eq. 7, the difference reflects greater λ_{rt} with increasing f_g (Eq. 8), at the onset of strong-foam generation.

In most cases, the strong foam exhibits up to a 150% increase in ∇p **(Fig. 4a)** and μ_{app} **(Fig. 4b)** in the decreasing v_t sequence compared with the increasing sequence; the hysteresis is stronger at lower f_g. Also, the strong foam shows shear-thinning behavior, with μ_{app} reduced by 1.5–3 times over a 100-fold increase in v_t.

The theory of Rossen and Gauglitz (1990) also predicts that ∇p required for mobilization of the strong foam is lower for low f_g. The prediction is supported by results in **Fig. 4**; ∇p shows a three- to fivefold decrease with decreasing f_g.

Fig. 5a presents the $\nabla p_{\text{gen}}^{\min}$ measurements vs. f_g in the 274-md core. $\nabla p_{\text{gen}}^{\min}$ and corresponding $v_{t,\text{gen}}^{\min}$ each again show a positive correlation with f_g. The values of $\nabla p_{\text{gen}}^{\min}$ fall within the range of 10^{-2}–10^{-1} bar/m (~0.04–0.44 psi/ft), one order of magnitude greater than in **Fig. 4a** with the 905-md core. The values of $v_{t,\text{gen}}^{\min}$ are also greater than in **Fig. 4a** and increase by a factor ~15 over the f_g range from 0.5 to 0.9. This suggests that foam generation in low-permeability media is more difficult; however, these values of $\nabla p_{\text{gen}}^{\min}$ still fall within a low range (<1 psi/ft), not a restriction to CO_2 foam generation deep in formations.

As in **Fig. 4**, strong foam exhibits similar hysteresis (50–150%) and shear-thinning (μ_{app} reduced by 1.5–5 times with increasing v_t, as shown in **Fig. 5b**). Nevertheless, unlike the monotonic dependence on f_g in **Fig. 4**, ∇p and μ_{app} in the strong-foam regime, in general,

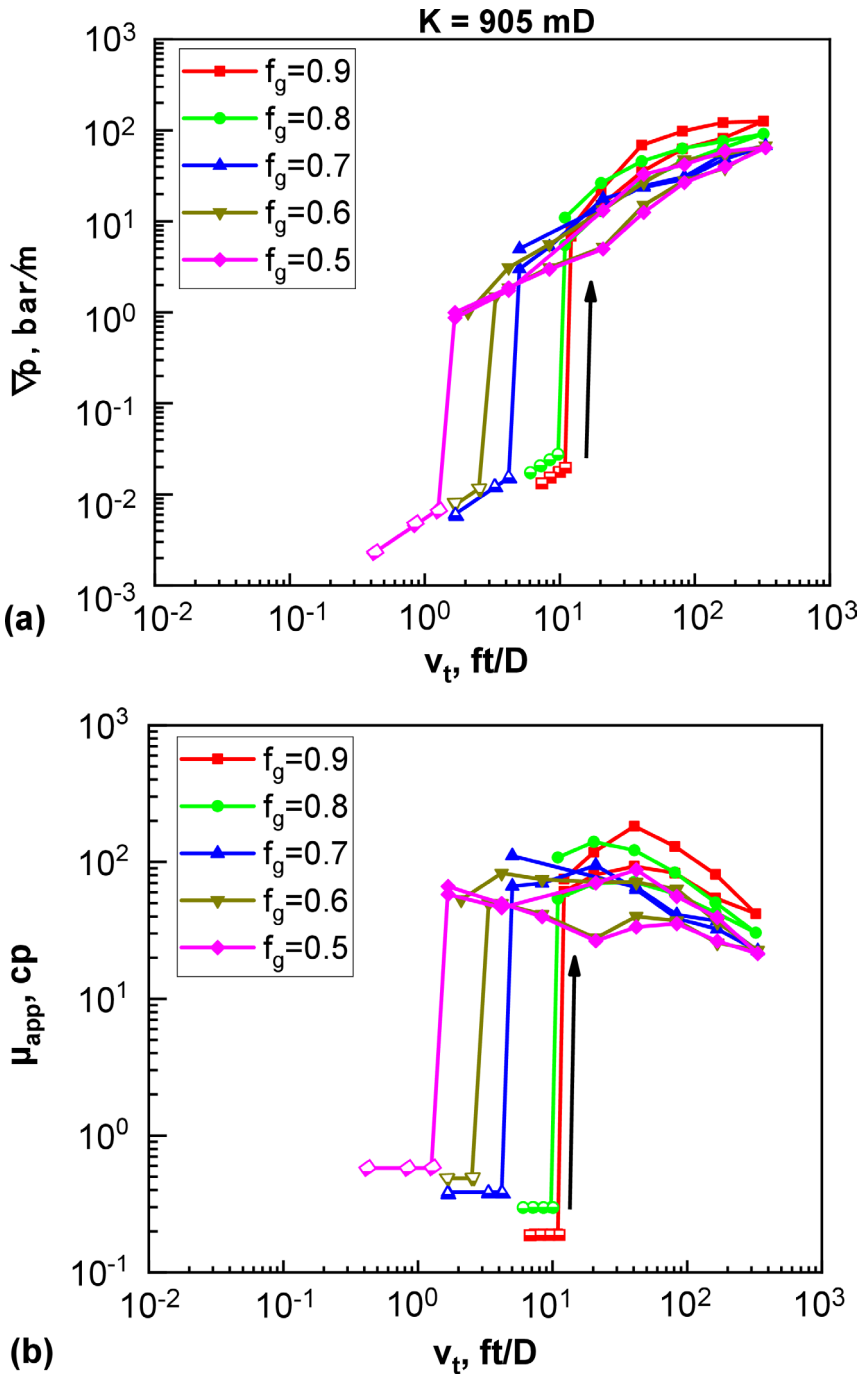

Fig. 4—(a) Pressure gradient ∇p (bar/m) and (b) apparent viscosity μ_{app} (cp) as a function of total interstitial velocity v_t (ft/D) in the core of 905 md, respectively, for various injected qualities f_g. In this plot and all subsequent plots, each curve represents steady ∇p measurements at constant f_g with C_s = 0.5 wt%, where v_t is imposed in the same increasing and then decreasing sequence as in Fig. 1b. Open symbols indicate points estimated from Darcy's law as in Fig. 3.

increase with f_g and then decrease. This could reflect the two flow regimes of strong foam (Alvarez et al. 2001; Kim et al. 2005; Tang et al. 2019a), where ∇p increases with f_g in the low-quality regime until a transition foam quality f_g^* and then decreases with f_g in the high-quality regime. Foam in a high-K medium is more stable and often has a greater value of f_g^* (Kapetas et al. 2017). In **Fig. 4** with greater K and thus greater f_g^*, all the f_g values examined are likely less than f_g^* (i.e., in the low-quality regime), resulting in ∇p monotonically increasing with f_g. In **Fig. 5** with lower K, f_g^* is likely in between the range of f_g examined, exhibiting nonmonotonic dependence of ∇p on f_g.

In the 27-md core **(Fig. 6a)**, ∇p_{gen}^{min} shows a similar increasing trend with f_g as in **Figs. 4a and 5a**. Nevertheless, the values of ∇p_{gen}^{min} are much greater than in **Figs. 4 and 5**, lying within the range of 5–15 bar/m (~22–66 psi/ft). Although this range is lower than for N_2 foam, it is still a challenge to be attained deep in a formation. Some factors in the field may help foam generation, such as formation heterogeneity and alternating injection of gas and liquid slugs. These factors could reduce the values of ∇p_{gen}^{min}, facilitating foam generation in low-K reservoirs and allowing for deep foam generation (Rossen 1999; Bertin et al. 1999; Li and Rossen 2005; Fernø et al. 2016; Skauge et al. 2020). In this case with lower K, strong foam exhibits nearly no hysteresis (as seen from the overlapping of the curves in the strong-foam regime in **Fig. 6a**) and strong shear-thinning rheology (as seen from μ_{app} in **Fig. 6b**).

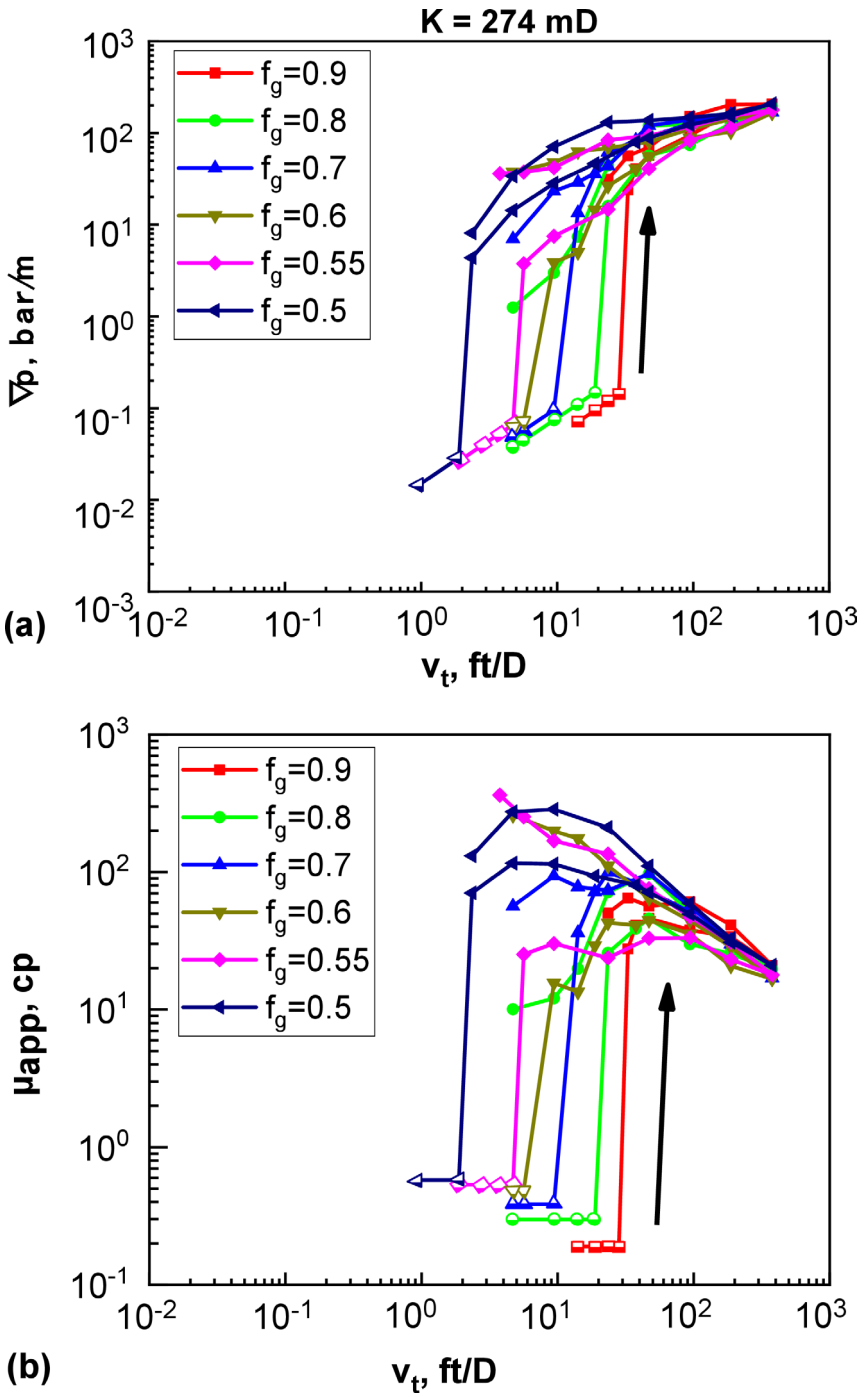

Fig. 5—(a) ∇p (bar/m) and (b) μ_{app} (cp) as a function of v_t (ft/D) in the core of 274 md, respectively, for various fixed f_g. Each curve is measured at steady state with a fixed f_g, where v_t is imposed in the same sequence as in Fig. 1b, and in all cases here C_s = 0.5 wt%. Open symbols indicate points estimated from Darcy's law as in Fig. 3.

Correlations between ∇p_{gen}^{min}, $v_{t,gen}^{min}$, and f_g. Fig. 7 plots a collection of the data on ∇p_{gen}^{min} and $v_{t,gen}^{min}$ as a function of f_g from **Figs. 4 through 6**. We then plot a linear fit to the data on log-log scale. The slopes of the fitted lines do not vary significantly with respect to K: 1.1, 2.5, and 2.1 in **Fig. 7a** for ∇p_{gen}^{min} vs. f_g and 3.9, 4.3, and 3.9 in **Fig. 7b** for $v_{t,gen}^{min}$ vs. f_g for 27 md, 274 md, and 905 md, respectively. This reveals that K has a mild impact on the correlations of ∇p_{gen}^{min} vs. f_g and of $v_{t,gen}^{min}$ vs. f_g.

Based on the average of the slopes, one can then approximate that ∇p_{gen}^{min} scales with f_g as $(f_g)^2$ for K ranging from 20 md to 1,000 md:

$$\nabla p_{gen}^{min} \sim (f_g)^2 . \quad (10)$$

Similarly, $v_{t,gen}^{min}$ approximately scales with f_g as $(f_g)^4$ for K = 20–1,000 md:

$$v_{t,gen}^{min} \sim (f_g)^4 . \quad (11)$$

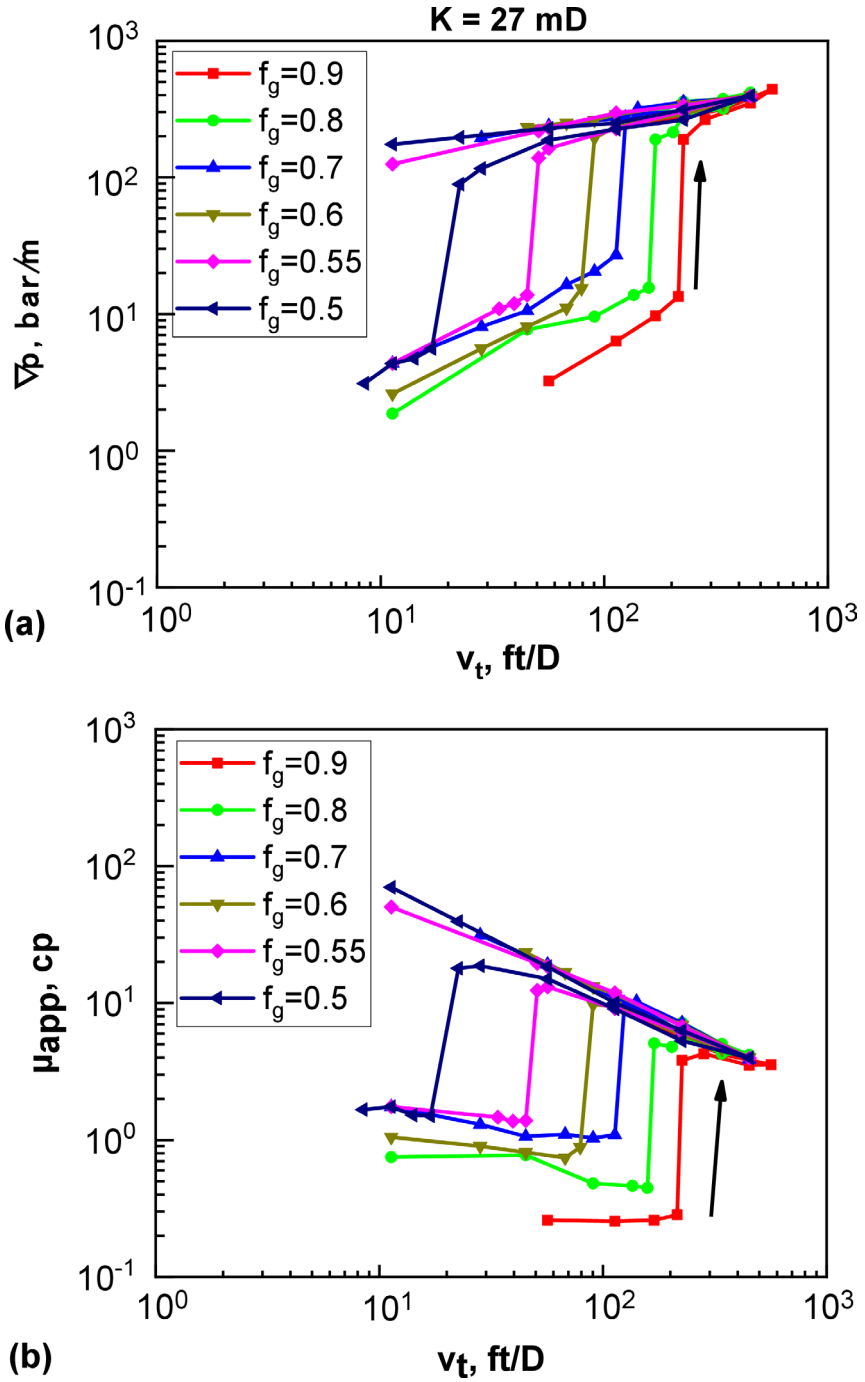

Fig. 6—(a) ∇p (bar/m) and (b) μ_{app} (cp) as a function of v_t (ft/D) in the core of 27 md, respectively, for various fixed f_g. Each curve represents steady ∇p measurements at constant f_g and C_s = 0.5 wt% with v_t imposed in an increasing and then decreasing sequence as in Fig. 1b.

The percolation theory of Rossen and Gauglitz (1990) reveals the physical mechanisms behind the positive correlation between ∇p_{gen}^{min} and f_g. With greater f_g in gas/liquid flow, there are fewer locations for lamella mobilization to start foam generation (i.e., fewer liquid-occupied pore throats blocking large stagnant clusters of gas-filled pores). In addition, increasing f_g results in greater capillary pressure, making stabilizing lamellae or lenses more difficult in the coarse-foam regime. As a result, at the onset of strong-foam generation, it requires a greater pressure gradient to mobilize those lamellae or lenses, thereby creating more lamellae by lamella division and snap-off.

Effect of Surfactant Concentration. Surfactant type and concentration (C_s) play a significant role in foam generation because the accumulation of lamellae depends on the stability of lamellae created. For C_s below the CMC, the dependence of lamella stability on C_s is especially severe. Moreover, below the CMC, surfactant concentration affects surface tension, thereby increasing the ease of mobilizing lamellae. The surfactant concentration deployed in the field is often relatively low (though far greater than the CMC), given the chemical cost. Moreover, deep in formations, C_s is limited by adsorption by rock and dilution by formation water. Here, we show how C_s affects foam generation at low concentrations, for low- and high-quality injection, respectively.

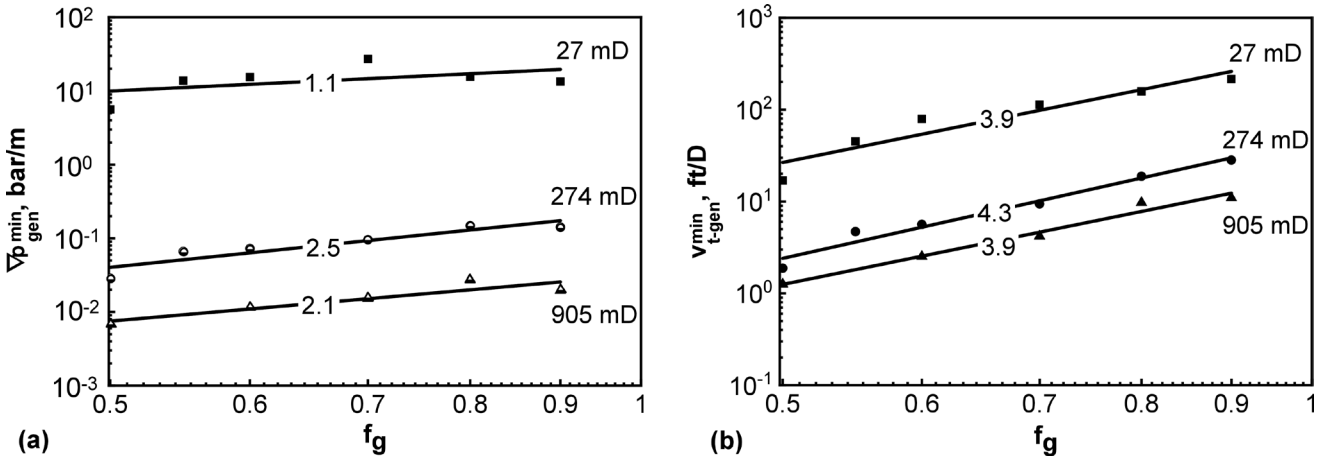

Fig. 7—(a) Minimum pressure gradient ∇p^{min}_{gen} and (b) minimum total interstitial velocity $v^{min}_{t,gen}$ for CO_2 foam generation as a function of foam quality f_g, respectively. The data here for ∇p^{min}_{gen} and $v^{min}_{t,gen}$ are taken from Figs. 4 through 6 (i.e., values of ∇p and v_t read off the curves just before the upward ∇p jump, corresponding to Point B in Fig. 1b). Numbers labeled on lines indicate the respective slopes in both (a) and (b).

Fig. 8a shows ∇p^{min}_{gen} measurements with respect to C_s, for low-quality injection in the 27-md core. Throughout these measurements, the injected quality f_g is fixed at 0.5, chosen such that the strong foam generated resides in the low-quality regime. The surfactant used here has a CMC ~0.09 wt% at the experimental conditions, and values of C_s examined range from 0.01 wt% to 0.5 wt%.

As in **Figs. 4a through 6a**, ∇p jumps abruptly when strong foam is triggered, and the magnitude of the jump is greater at higher C_s. For $C_s \geq$ CMC, as one expects, both ∇p^{min}_{gen} and $v^{min}_{t,gen}$ show a decreasing trend with increasing C_s. The impact of C_s on the critical thresholds for foam generation above the CMC, however, is mild. For a 10-fold increase in C_s from 0.05 wt% to 0.5 wt%, ∇p^{min}_{gen} decreases by a factor less than 2 and $v^{min}_{t,gen}$ by a factor about 3.

With C_s = 0.01 wt% < CMC (black curves in **Fig. 8a**), ∇p shows a continuous, though steep, increase with increasing v_t, instead of a jump as indicated in **Fig. 1b**. Similar behavior was reported by Kibodeaux (1997). The values of μ_{app} (black curve) in **Fig. 8b** reflect the presence of very coarse foam, as seen from μ_{app} = 1 cp to 1.5 cp, slightly greater than 0.58 cp estimated from Darcy's law for no foam.

Fig. 9a presents ∇p^{min}_{gen} measurements with various C_s at fixed f_g = 0.9. With high-quality injection, foam generation is more sensitive to C_s. For f_g = 0.9 in **Fig. 9a**, ∇p^{min}_{gen} drops by 3-fold over a 5-fold increase in C_s, compared with 2-fold over a 10-fold increase in C_s at f_g = 0.5 in **Fig. 8a**. Also, C_s that is required for triggering strong foam is greater for high-quality injection. This can be seen from the ∇p jump: for f_g = 0.9 in **Fig. 9a**, the jump occurs at a limit $C_s \geq$ 0.1 wt%, while for f_g = 0.5 in **Fig. 8a**, the jump occurs at a lower limit, $C_s \geq$ 0.05 wt%.

The results in **Fig. 8** (black curve) and **Fig. 9** (black and orange curves) reveal that a minimum surfactant concentration (e.g., the CMC) may be needed to trigger a jump to strong foam, with greater required concentration at higher f_g. The minimum C_s required for strong-foam generation could be easily met in the near-well region since C_s injected is usually much greater than the CMC. At a long distance away from the injection well due to surfactant adsorption by rocks and dilution by formation water, C_s at the displacement front may fall below the CMC, restricting foam generation deep in formations. In the cases where no strong foam is triggered (no ∇p jump occurs with increasing v_t), foam at very low values of C_s still maintains some strength in the decreasing v_t sequence. In **Fig. 9**, the foam for C_s = 0.01 wt% and 0.05 wt% upon reducing v_t is nearly as strong as the cases with a distinct trigger for foam generation. This is not true for C_s = 0.01 wt% in **Fig. 8**. The mechanism for this behavior is unclear. Strong foam is created as velocity increases for these lowest surfactant concentrations but, gradually, not as a distinct jump. The mechanism for this is not clear.

Correlations between ∇p^{min}_{gen}, $v^{min}_{t,gen}$, and C_s. Fig. 10 plots ∇p^{min}_{gen} and $v^{min}_{t,gen}$ against C_s, respectively. The data in **Fig. 10** are taken from **Figs. 8 and 9**. Solid lines represent a linear fitting to the data on log-log scale. The slopes of the linear lines do not change greatly with f_g from 0.5 to 0.9. Based on the average of the slopes, one can get an approximate correlation for ∇p^{min}_{gen} vs. C_s:

$$\nabla p^{min}_{gen} \sim (C_s)^{-0.4}, \quad (12)$$

where the slopes in **Fig. 10a** are about 0.2 at f_g = 0.5 and −0.6 at f_g = 0.9. Similarly, $v^{min}_{t,gen}$ vs. C_s follows an approximate correlation:

$$v^{min}_{t,gen} \sim (C_s)^{-0.4}, \quad (13)$$

where the slopes in **Fig. 10b** are about −0.5 at f_g = 0.5 and −0.2 at f_g = 0.9.

Similar to the effect of f_g, the mechanism behind the correlation between ∇p^{min}_{gen} and C_s reflects the impact of C_s on capillary pressure and lamella/lens stability in the coarse-foam regime. A lower surfactant concentration means less stable lamellae. The triggering of strong-foam generation is a dynamic process that results from mobilization of lamellae and depends on lamellae surviving mobilization. With low C_s, it then requires a greater pressure gradient to mobilize more lamellae/lenses so that enough survive to create more lamellae by lamella division and snap-off.

Effect of Permeability: Comparison between CO_2 and N_2 Foams. Fig. 11 compares the ∇p^{min}_{gen} data as a function of K between CO_2 (filled symbols) and N_2 (open symbols) foams. The data with CO_2 are from this study in artificial consolidated sandstone and from Gauglitz et al. (2002) in Boise sandstone (f_g = 0.8). The data with N_2 (f_g = 0.9) are from Gauglitz et al., mostly in sand/bead packs, with

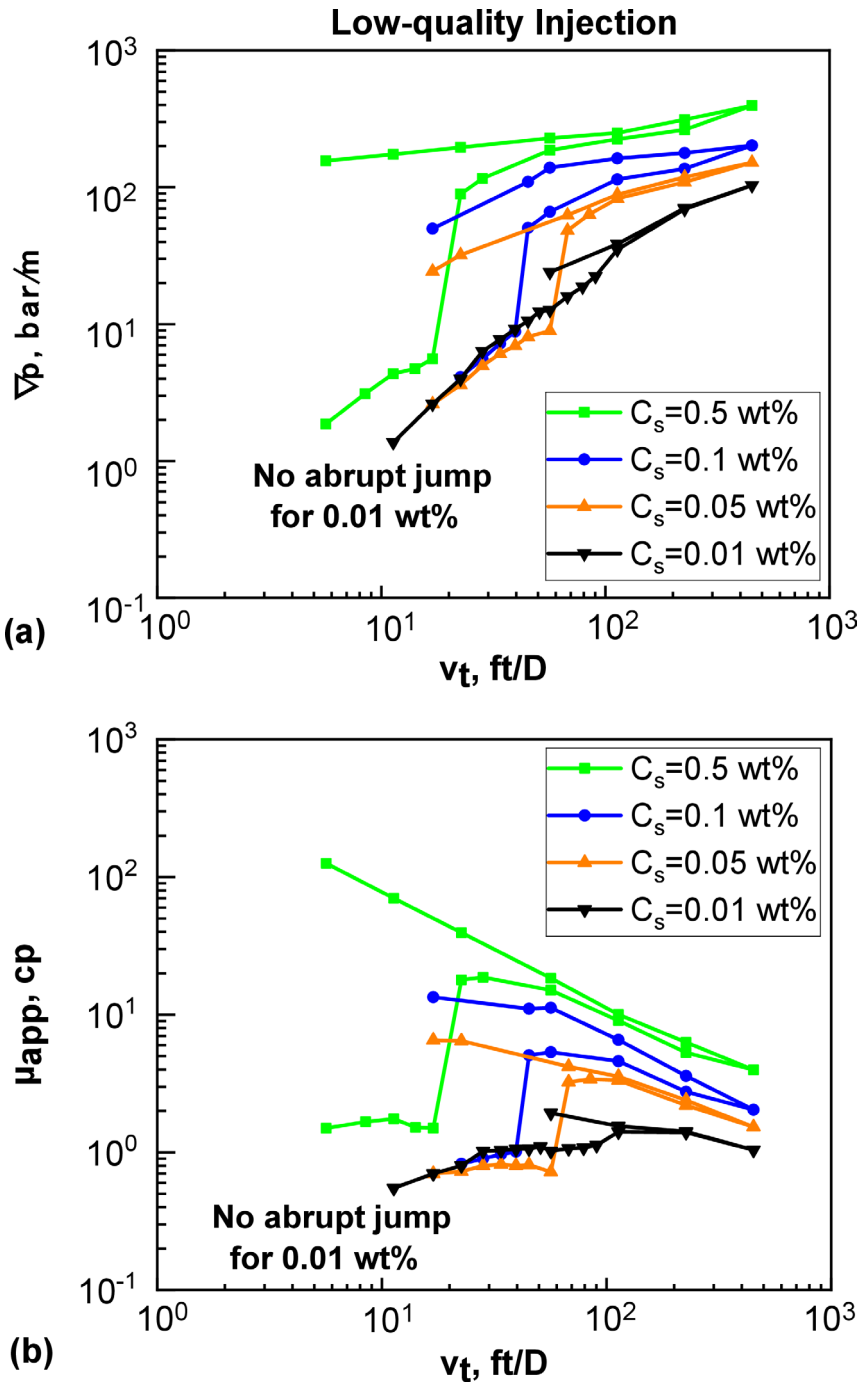

Fig. 8—(a) ∇p (bar/m) and (b) μ_{app} (cp) as a function of v_t (ft/D) in the 27-md core, respectively, with respect to surfactant concentration C_s for low-quality injection. For all cases of C_s examined here, the injected quality is fixed at f_g = 0.5.

some data from outcrop rock cores. The solid lines represent a linear fit to the data in each case on log-log scale. Our CO_2 foam data have some variations depending on injected quality f_g. The differences in porous media complicate the comparison between N_2 and CO_2.

The values of ∇p_{gen}^{min} for CO_2 foam are two to three orders of magnitude less than for N_2 foam in the K range where they overlap. The lower ∇p_{gen}^{min} for CO_2 partly arises from the lower surface tension for supercritical CO_2 surfactant than for N_2 surfactant (Farajzadeh et al. 2009). This suggests that deep in formations with limited ∇p, long-distance propagation is much less an issue for CO_2 foam than for N_2 foam.

The reduction in ∇p_{gen}^{min} is much greater than the difference in surface tensions. There is as yet no complete explanation for this. CO_2 foam can also flow at much lower pressure gradient than N_2 foam (e.g., Farajzadeh et al. 2009). It has been suggested that this indicates that CO_2 foam is less stable than N_2 foam (Zeng et al. 2016), but this would work against easier foam generation. The lower surface tension suggests that capillary pressure may be lower in CO_2 foam than N_2 foam; this would help bubbles to flow more easily (Hirasaki and Lawson 1985). Supercritical CO_2 is more viscous than N_2. This suggests that at the same f_g, gas saturation would be larger for CO_2 than

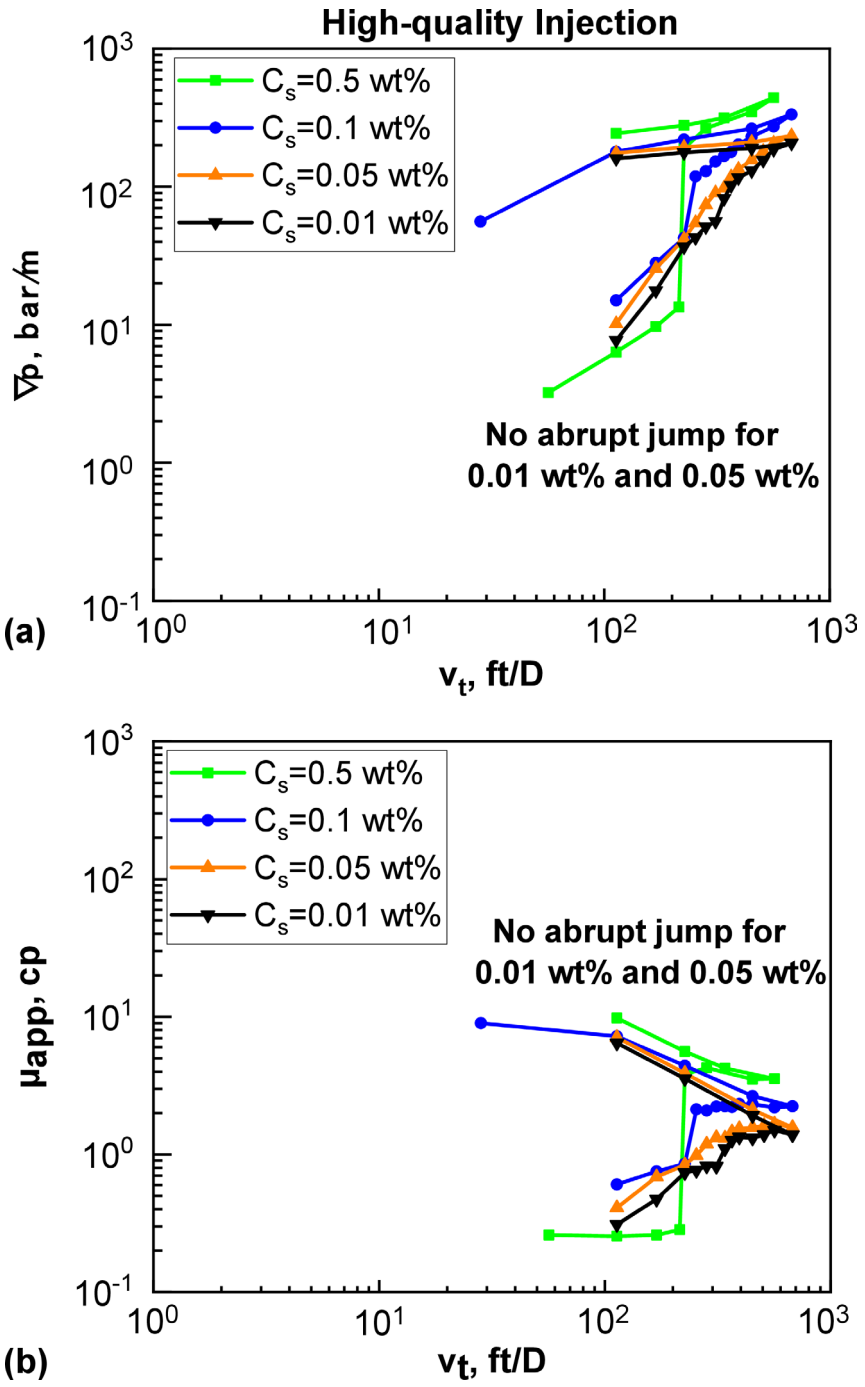

Fig. 9—(a) ∇p (bar/m) and (b) μ_{app} (cp) as a function of v_t (ft/D) in the 27-md core, respectively, with respect to surfactant concentration C_s for high-quality injection. For all cases of C_s examined here, the injected quality is fixed at f_g = 0.9.

N_2. According to theory (Fig. 9 of Rossen and Gauglitz 1990), this could hinder foam generation. A complete explanation must await further research.

The data with N_2 in homogeneous sand/bead packs (upper right in **Fig. 11**) are in good agreement with the correlation in Eq. 1, showing that ∇p_{gen}^{min} scales with permeability as K^{-1}. The data with CO_2 in consolidated sandstone (lower left in **Fig. 11**) show, however, that ∇p_{gen}^{min} scales roughly with K as K^{-2}:

$$\nabla p_{gen}^{min} \sim K^{-2}. \quad (14)$$

The different powers in the correlations of Eqs. 1 through 14 may arise from several factors that are different between the experiments. The correlations between ∇p_{gen}^{min}, pore geometry, and K are more complex in consolidated media than assumed in the theory of Rossen and Gauglitz (1990). Gas type and surfactant formulation and their effects on surface tension may also play a role in the different behavior of ∇p_{gen}^{min} with K.

Fig. 12 shows the correlation of minimum total interstitial velocity $v_{t,gen}^{min}$ with permeability K on log-log scale. The values of $v_{t,gen}^{min}$ are more sensitive to injected quality f_g, in comparison with ∇p_{gen}^{min} **(Fig. 11)**. Also, $v_{t,gen}^{min}$ for CO_2 foam is about one order of magnitude lower than for N_2 foam at same qualities.

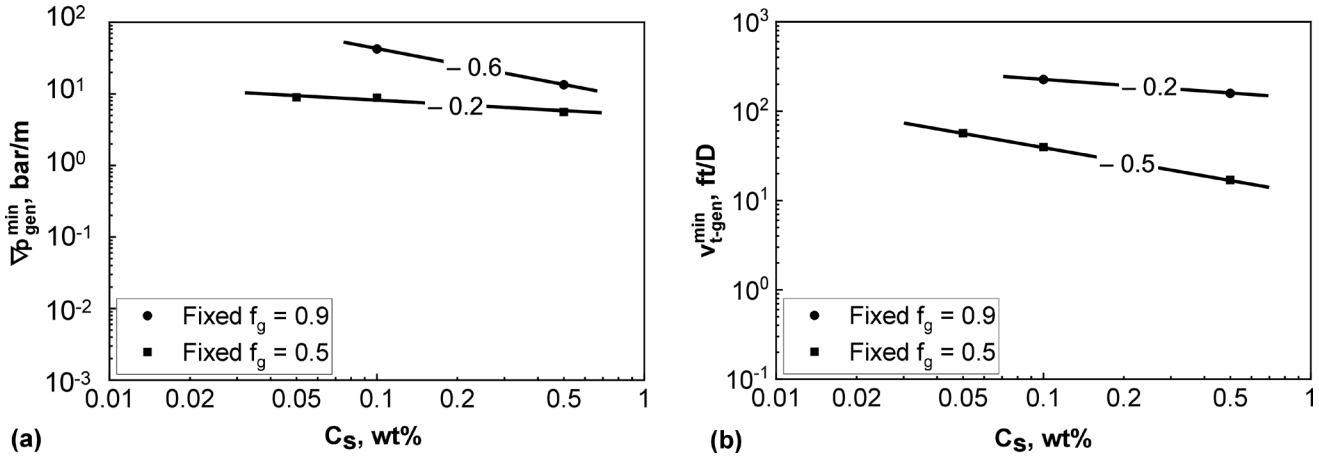

Fig. 10—(a) Minimum pressure gradient ∇p^{min}_{gen} and (b) minimum total interstitial velocity $v^{min}_{t,gen}$ for CO_2 foam generation as a function of surfactant concentration C_s, respectively. The data here for ∇p^{min}_{gen} and $v^{min}_{t,gen}$ are values of ∇p and v_t observed just before the ∇p jump in Figs. 7 through 8, corresponding to Point B in Fig. 1b. Numbers labeled on lines indicate the respective slopes in both (a) and (b).

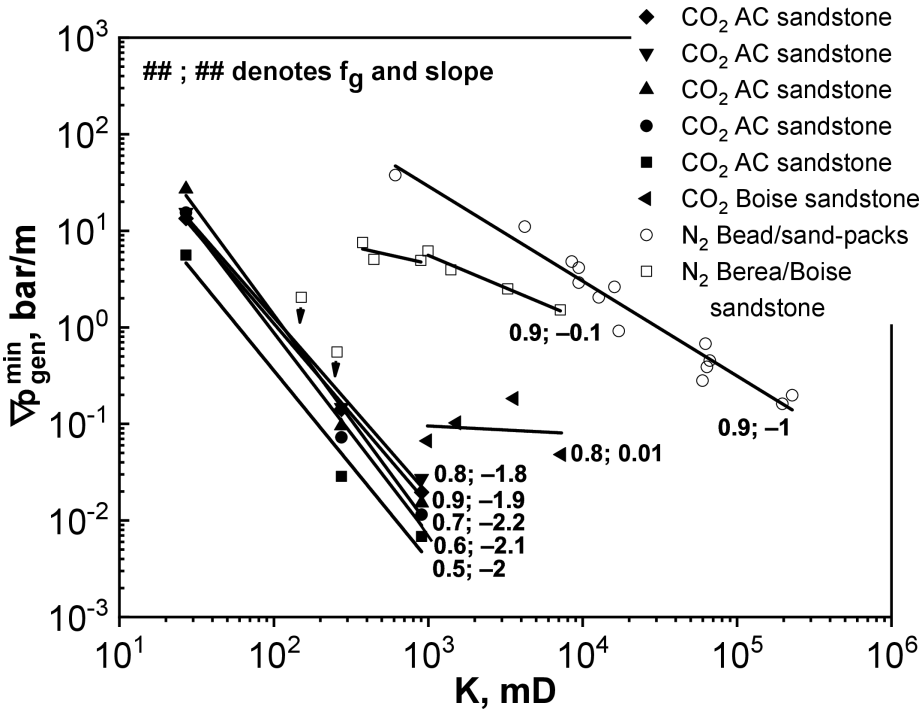

Fig. 11—Comparison of ∇p^{min}_{gen} as a function of permeability K between CO_2 and N_2 foams. AC in the legend denotes artificial consolidated sandstone. Filled symbols represent the data for CO_2 and open symbols for N_2, and solid lines are linear fit to the data. The numbers labeled indicate injected quality f_g and line slope in each case. The CO_2 foam data in Boise sandstone and all the N_2 foam data are taken from Gauglitz et al. (2002).

Our data with CO_2 in artificial consolidated sandstone show that $v^{min}_{t,gen}$ scales with K approximately as K^{-1}:

$$v^{min}_{t,gen} \sim K^{-1}. \quad (15)$$

The power in Eq. 15 is an average of the slopes of the lines with our data in **Fig. 12**. Based on Eq. 7, $v^{min}_{t,gen}$ is a function of both permeability and total relative mobility. The CO_2 data in Boise sandstone from Gauglitz et al. (2002) give $v^{min}_{t,gen}$ scaling as $K^{-0.6}$, but they report substantial uncertainty in their data, and the data are very limited.

The data of Gauglitz et al. (2002) show that with N_2, $v^{min}_{t,gen}$ is nearly independent of K, when ∇p^{min}_{gen} scales as K^{-1} as in Eq. 1. The data of Yu et al. (2020) are collected in Bentheimer sandstone of 2.5 darcies only, which are not sufficient to indicate the trend of $v^{min}_{t,gen}$ vs. K. Thus, more research is needed to verify the correlations between $v^{min}_{t,gen}$ and K for both CO_2 and N_2.

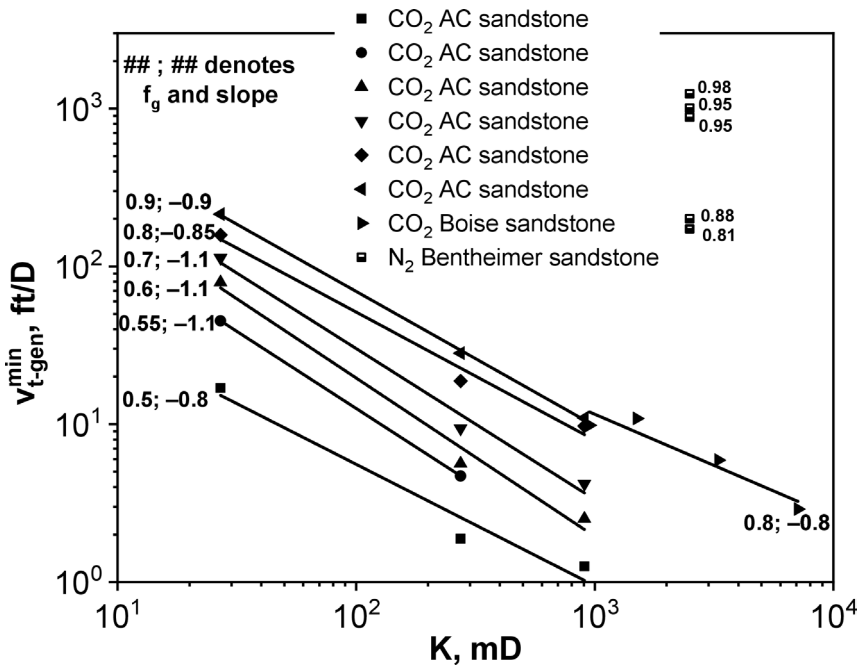

Fig. 12—Minimum total interstitial velocity $v_{t,\mathrm{gen}}^{\mathrm{min}}$ (ft/D) for foam generation as a function of *K* (md). All the CO_2 data are from our experiments in Figs. 4 through 6, except for those in Boise sandstone from Gauglitz et al. (2002) and N_2 data (open symbols) from Yu et al. (2020). AC in the legend denotes artificial consolidated sandstone. Solid lines represent linear fitting to the data. Labeled numbers indicate injected quality f_g and line slope in each case.

Discussion

For the first time, we experimentally determine the critical thresholds for CO_2 foam generation in terms of $\nabla p_{\mathrm{gen}}^{\mathrm{min}}$ and $v_{t,\mathrm{gen}}^{\mathrm{min}}$ and their quantitative correlations with factors f_g, C_s, and K. Nevertheless, given the limited data, the fitted correlations in Eqs. 10 through 14 are subject to uncertainty. Before applying these correlations to predict the conditions for CO_2 foam generation, it is necessary to collect more data for further verification.

Also, in this initial study, we address one of the two processes governing foam propagation (i.e., foam generation at the displacement front). The other process, convection of generated foam, cannot be quantified with straight cores. This is because once strong foam is triggered, foam erupts instantly throughout a core, yielding a ∇p (Point C in **Fig. 1b**) greater than $\nabla p_{\mathrm{prop}}^{\mathrm{min}}$ (Point E in **Fig. 1b**) for its propagation. As a result, one cannot determine the critical value of $\nabla p_{\mathrm{prop}}^{\mathrm{min}}$, below which foam does not propagate as it moves forward. In our next study, we would use a variable diameter core to determine $\nabla p_{\mathrm{prop}}^{\mathrm{min}}$ for CO_2 foam propagation. A core with diameter increasing in the flow direction makes an abrupt decrease in superficial velocity and pressure gradient along the core. This special design allows for determining whether foam generated upstream with high ∇p can propagate into next sections with low ∇p and thus the critical value of $\nabla p_{\mathrm{prop}}^{\mathrm{min}}$; a similar procedure is reported in Yu et al. (2020).

All our experiments here are conducted with steady coinjection of gas and liquid into homogeneous porous media. Data in the literature demonstrate that the formation heterogeneity (Almajid et al. 2019; Shah et al. 2019), in particular, flow across layer boundaries, and alternating injection of gas and liquid slugs (Kovscek and Radke 1994; Rossen 1996) facilitates foam generation. However, the quantitative correlations between these factors and $\nabla p_{\mathrm{gen}}^{\mathrm{min}}$ are still ambiguous. For instance, the data with CO_2 in Boise sandstone in **Fig. 11** show that $\nabla p_{\mathrm{gen}}^{\mathrm{min}}$ is nearly independent of K, instead of scaling as a power function of K. Nevertheless, Gauglitz et al. (2002) report substantial uncertainty in those data, so further research is needed to demonstrate whether $\nabla p_{\mathrm{gen}}^{\mathrm{min}}$ is truly independent of K in heterogeneous formations. In addition, to the best of our knowledge, no data are reported on the impact of heterogeneity and alternating slug injection on the propagation threshold $\nabla p_{\mathrm{prop}}^{\mathrm{min}}$ for CO_2 foam. More research is needed to predict the conditions for long-distance propagation of CO_2 foam under those complex conditions. This is especially crucial in evaluating the potential and optimizing the design of foam-assisted carbon sequestration processes.

We estimate $\nabla p_{\mathrm{gen}}^{\mathrm{min}}$ for the two higher-permeability cores using foam-free relative permeability functions. There can be some mobility reduction in the coarse-foam state before strong-foam generation is triggered. For the two foam qualities $f_g = 0.6$ and 0.9, the apparent viscosity measured for the 27-md core at the onset of strong-foam generation is 1.8 and 1.25 times that we estimated based on relative permeability curves, respectively **(Figs. 4 through 6)**. The difference is modest and would not substantially alter our conclusions.

Our experiments were conducted under conditions ideal for strong foam—relatively low temperature and salinity, water-wet rock, and absence of oil. Under more realistic field conditions, the pressure gradients may be lower (and the foam weaker). Further investigation into the effects of wettability and presence of residual oil is needed to determine these effects.

Conclusions

In steady coinjection (not drainage), CO_2 foam exhibits a minimum pressure gradient ($\nabla p_{\mathrm{gen}}^{\mathrm{min}}$) or minimum total interstitial velocity ($v_{t,\mathrm{gen}}^{\mathrm{min}}$) beyond which strong-foam generation is triggered, featuring a sudden, abrupt increase in ∇p.

Our results show the effects on $\nabla p_{\mathrm{gen}}^{\mathrm{min}}$ and $v_{t,\mathrm{gen}}^{\mathrm{min}}$ of injected quality (f_g), surfactant concentration (C_s), and permeability (K). The data reveal that conditions that help stabilize lamellae reduce the values of $\nabla p_{\mathrm{gen}}^{\mathrm{min}}$ and $v_{t,\mathrm{gen}}^{\mathrm{min}}$, facilitating foam generation. Thus, $\nabla p_{\mathrm{gen}}^{\mathrm{min}}$ and $v_{t,\mathrm{gen}}^{\mathrm{min}}$ increase with increasing f_g, decrease with increasing C_s, and decrease with increasing K. Specifically,

- $\nabla p_{\text{gen}}^{\text{min}}$ scales with f_g as $(f_g)^2$; $v_{t,\text{gen}}^{\text{min}}$ scales with f_g as $(f_g)^4$.
- Both $\nabla p_{\text{gen}}^{\text{min}}$ and $v_{t,\text{gen}}^{\text{min}}$ scale with C_s as $(C_s)^{-0.4}$.
- $\nabla p_{\text{gen}}^{\text{min}}$ scales with K as K^{-2}, in comparison with K^{-1} for N_2 foam.
- $v_{t,\text{gen}}^{\text{min}}$ scales with K as K^{-1}, in contrast to N_2 foam with $v_{t,\text{gen}}^{\text{min}}$ nearly independent of K, upon $\nabla p_{\text{gen}}^{\text{min}}$ scaling as K^{-1}.

These correlations are subject to uncertainty, given the limited data; more data are needed for further verification of these correlations.

At very low C_s, foam generation shows a continuous, though steep, increase in ∇p with increasing v_t, instead of an abrupt jump in ∇p. This suggests that a minimum C_s (e.g., the CMC) may be needed to trigger strong-foam generation.

In the cores with $K \geq 274$ md, $\nabla p_{\text{gen}}^{\text{min}}$ is less than 0.17 bar/m (0.75 psi/ft), easily attainable throughout a formation. This is two to three orders of magnitude less than $\nabla p_{\text{gen}}^{\text{min}}$ for N_2, suggesting long-distance foam propagation with CO_2 is much less an issue than with N_2.

CO_2 foam generation in low-permeability media could be challenging, as seen from $\nabla p_{\text{gen}}^{\text{min}}$ ~10 bar/m (42 psi/ft) in the 27-md core. However, certain factors (e.g., formation heterogeneity and alternating injection of gas and liquid slugs) may reduce the values of $\nabla p_{\text{gen}}^{\text{min}}$ and help foam generation in low-permeability formations.

N_2 data (Yu et al. 2020) reveal that $\nabla p_{\text{prop}}^{\text{min}}$ required for foam propagation is much greater than $\nabla p_{\text{gen}}^{\text{min}}$ for its generation, whereas the corresponding magnitude of $\nabla p_{\text{prop}}^{\text{min}}$ with CO_2 is still unknown. More research is needed to quantify these conditions for CO_2 foam generation and propagation as well as the impact of permeability, heterogeneity, and injection strategy.

Further research with a variety of surfactants tailored to a wide range of reservoir conditions is desirable and an essential extension of this study.

Acknowledgment

This project is funded by the Open Fund (PLN2022-01) of State Key Laboratory of Oil and Gas Reservoir Geology and Exploitation (Southwest Petroleum University) and the United Arab Emirates University Research Grant (12N099).

References

Al-Homadhi, E. S. 2002. Artificial Sandstone Cores Production with a Wide Range of Petrophysical Properties. *J King Saud Univ Eng Sci* **14** (1): 95–117. https://doi.org/10.1016/S1018-3639(18)30747-5.

Almajid, M. M., Nazari, N., and Kovscek, A. R. 2019. Modeling Steady-State Foam Flow: Hysteresis and Backward Front Movement. *Eng Fuels* **33** (11): 11353–11363. https://doi.org/10.1021/acs.energyfuels.9b01842.

Alvarez, J. M., Rivas, H. J., and Rossen, W. R. 2001. Unified Model for Steady-State Foam Behavior at High and Low Foam Qualities. *SPE J.* **6** (3): 325–333. https://doi.org/10.2118/74141-PA.

Ashoori, E., Marchesin, D., and Rossen, W. R. . R. 2012. Multiple Foam States and Long-Distance Foam Propagation in Porous Media. *SPE J.* **17** (4): 1231–1245. https://doi.org/10.2118/154024-PA.

Bertin, H. J., Apaydin, O. G., Castanier, L. M. et al. 1999. Foam Flow in Heterogeneous Porous Media: Effect of Cross Flow. *SPE J.* **4** (2): 75–82. https://doi.org/10.2118/56009-PA.

Bird, R. B., Stewart, W. E., and Lightfoot, E. N. 2002. *Transport Phenomena*, second edition. New York: Wiley.

Chou, S. I. 1991. Conditions for Generating Foam in Porous Media. Paper presented at the SPE Annual Technical Conference and Exhibition, Dallas, Texas, Texas, 6−9 October. https://doi.org/10.2118/22628-MS.

Eftekhari, A. A. and Farajzadeh, R. 2017. Effect of Foam on Liquid Phase Mobility in Porous Media. *Sci Rep* **7**. https://doi.org/10.1038/srep43870.

Farajzadeh, R., Andrianov, A., Bruining, H. et al. 2009. Comparative Study of CO_2 and N_2 Foams in Porous Media at Low and High Pressure−Temperatures. *Ind Eng Chem* (9): 4542–4552. https://doi.org/10.1021/ie801760u.

Farajzadeh, R., Andrianov, A., Krastev, R. et al. 2012. Foam-Oil Interaction in Porous Media: Implications for Foam Assisted Enhanced Oil Recovery. *Adv Colloid Interface Sci* **183–184**: 1–13. https://doi.org/10.1016/j.cis.2012.07.002.

Fernø, M. A., Gauteplass, J. ., Pancharoen, M. . et al. 2016. Experimental Study of Foam Generation, Sweep Efficiency, and Flow in a Fracture Network. *SPE J.* **21** (4): 1140–1150. https://doi.org/10.2118/170840-PA.

Gauglitz, P. A., Friedmann, F., I. Kam, S. et al. 2002. Foam Generation in Homogeneous Porous Media. *Chem Eng Sci* **57** (19): 4037–4052. https://doi.org/10.1016/S0009-2509(02)00340-8.

Hirasaki, G. J. and Lawson, J. B. 1985. Mechanisms of Foam Flow in Porous Media: Apparent Viscosity in Smooth Capillaries. *SPE J.* **25** (2): 176–190. https://doi.org/10.2118/12129-PA.

Jishun, Q. 2004. The Manufacture and Use of Artificial Consolidated Core Samples in China, Research Institute of Petroleum Exploration and Development, PetroChina. Paper presented at the International Symposium of the Society of Core Analysts, Abu Dhabi, UAE, 5−9 October.

Kam, S. I. 2008. Improved Mechanistic Foam Simulation with Foam Catastrophe Theory. *Colloids Surf A: Physicochem Eng Aspects* **318** (1–3): 62–77. https://doi.org/10.1016/j.colsurfa.2007.12.017.

Kam, S. I. and Rossen, W. R. 2002. A Model for Foam Generation in Homogeneous Media. Paper presented at the SPE Annual Technical Conference and Exhibition, San Antonio, Texas, 29 September−2 October. https://doi.org/10.2118/77698-MS.

Kapetas, L., Vincent Bonnieu, S., Farajzadeh, R. et al. 2017. Effect of Permeability on Foam-Model Parameters: An Integrated Approach from Core-Flood Experiments through to Foam Diversion Calculations. *Colloids Surf A: Physicochem Eng Aspects* **530**: 172–180. https://doi.org/10.1016/j.colsurfa.2017.06.060.

Kibodeaux, K. 1997. *Experimental and Theoretical Studies of Foam Mechanisms in Enhanced Oil Recovery and Matrix Acidization Applications*. PhD Dissertation, University of Texas at Austin, Austin, Texas, USA.

Kim, J. S., Dong, Y., and Rossen, W. R. 2005. Steady-State Flow Behavior of CO_2 Foam. *SPE J.* **10** (4): 405–415. https://doi.org/10.2118/89351-PA.

Kovscek, A. R. and Radke, C. J. 1994. Fundamentals of Foam Transport in Porous Media. In *Foams: Fundamentals and Applications in the Petroleum Industry*, ed. L. L. Schramm, 115–163. Washington, D.C., USA: ACS Advances in Chemistry Series. https://doi.org/10.1021/ba-1994-0242.ch003.

Li, Q. and Rossen, W. R. 2005. Injection Strategies for Foam Generation in Homogeneous and Layered Porous Media. Paper presented at the SPE Annual Technical Conference and Exhibition, Dallas, Texas, USA, 9−12 October. https://doi.org/10.2118/96116-MS.

Lotfollahi, M., Kim, I., Beygi, M. R. et al. 2017. Foam Generation Hysteresis in Porous Media: Experiments and New Insights. *Transp Porous Med* **116** (2): 687–703. https://doi.org/10.1007/s11242-016-0796-6.

Ransohoff, T. C. and Radke, C. J. 1988. Mechanisms of Foam Generation in Glass-Bead Packs. *SPE Res Eng* **3** (2): 573–585. https://doi.org/10.2118/15441-PA.

Rossen, W. R. and Gauglitz, P. A. 1990. Percolation Theory of Creation and Mobilization of Foams in Porous Media. *AIChE Journal* **36** (8): 1176–1188. https://doi.org/10.1002/aic.690360807.

Rossen, W. R. 2003. A Critical Review of Roof Snap-off as A Mechanism of Steady-State Foam Generation in Homogeneous Porous Media. *Colloids Surf A: Physicochem Eng Aspects* **225** (1–3): 1–24. https://doi.org/10.1016/S0927-7757(03)00309-1.

Rossen, W. R., Farajzadeh, R., Hirasaki, G. J. et al. 2024. Potential and Challenges of Foam-Assisted CO_2 Sequestration. *Geoenergy Sci Eng* **239**: 212929. https://doi.org/10.1016/j.geoen.2024.212929.

Rognmo, A. U., Heldal, S., and Fernø, M. A. 2018. Silica Nanoparticles to Stabilize CO_2-Foam for Improved CO_2 Utilization: Enhanced CO_2 Storage and Oil Recovery from Mature Oil Reservoirs. *Fuel* **216**: 621–626. https://doi.org/10.1016/j.fuel.2017.11.144.

Rossen, W. R. 1996. Foams in Enhanced Oil Recovery. In *Foams: Theory, Measurements and Applications*, eds. R. K. Prud'homme and S. Khan, 413–464. New York: Routledge. https://doi.org/10.1201/9780203755709.

Rossen, W. R. 1999. Foam Generation at Layer Boundaries in Porous Media. *SPE J.* **4** (4): 409–412. https://doi.org/10.2118/59395-PA.

Shah, S. Y., Wolf, K.-H., Pilus, R. M. et al. 2019. Foam Generation by Capillary Snap-Off in Flow Across a Sharp Permeability Transition. *SPE J.* **24** (1): 116–128. https://doi.org/10.2118/190210-PA.

Skauge, A., Solbakken, J., Ormehaug, P. A. et al. 2020. Foam Generation, Propagation and Stability in Porous Medium. *Transp Porous Med* **131** (1): 5–21. https://doi.org/10.1007/s11242-019-01250-w.

Tang, J., Vincent-Bonnieu, S., and Rossen, W. R. 2019a. Experimental Investigation of the Effect of Oil on Steady-State Foam Flow in Porous Media. *SPE J.* **24** (1): 140–157. https://doi.org/10.2118/194015-PA.

Tang, J., Vincent-Bonnieu, S., and Rossen, W. R. 2019b. CT Coreflood Study of Foam Flow for Enhanced Oil Recovery: The Effect of Oil Type and Saturation. *Energy* **188**. https://doi.org/10.1016/j.energy.2019.116022.

Tanzil, D., Hirasaki, G. J., and Miller, C. A. 2000. Mobility of Foam in Heterogeneous Media: Flow Parallel and Perpendicular to Stratification. *SPE J.* **7** (2): 203–212. https://doi.org/10.2118/78601-PA.

Tanzil, D., Hirasaki, G. J., and Miller, C. A. 2002. Conditions for Foam Generation in Homogeneous Porous Media. Paper presented at the SPE/DOE Improved Oil Recovery Symposium, Tulsa, Oklahoma, USA, 13−17 April. https://doi.org/10.2118/75176-MS.

Wang, H., Liu, Y., Song, Y. et al. 2012. Fractal Analysis and Its Impact Factors on Pore Structure of Artificial Cores Based on the Images Obtained Using Magnetic Resonance Imaging. *J Appl Geophy* **86**: 70–81. https://doi.org/10.1016/j.jappgeo.2012.07.015.

Yu, G. and Rossen, W. R. 2022. Simulation Models for the Minimum Velocity for Foam Generation and Propagation. *J Pet Sci Eng* **214**: 110406. https://doi.org/10.1016/j.petrol.2022.110406.

Yu, G., Vincent-Bonnieu, S., and Rossen, W. R. 2020. Foam Propagation at Low Superficial Velocity: Implications for Long-Distance Foam Propagation. *SPE J.* **25** (6): 3457–3471. https://doi.org/10.2118/201251-PA.

Zeeman, E. C. 1977. *Catastrophe Theory: Selected Papers*, 1972–1977. Boston, Massachusetts, USA: Addison-Wesley.

Zeng, Y., Farajzadeh, R., Eftekhari, A. A. et al. 2016. Role of Gas Type on Foam Transport in Porous Media. *Langmuir* **32** (25): 6239–6245. https://doi.org/10.1021/acs.langmuir.6b00949.